Combustion and Flame 178 (2017) 148–157

Contents lists available at ScienceDirect

Combustion and Flame

journal homepage: www.elsevier.com/locate/combustflame

Experimental investigation on spark ignition of annular premixed combustors

Edouard Machover*, Epaminondas Mastorakos

Department of Engineering, University of Cambridge, Cambridge CB2 1PZ, UK

ARTICLE INFO

Article history:
Received 25 April 2016
Revised 12 July 2016
Accepted 17 January 2017

Keywords:
Gas turbines
Spark ignition
Premixed flames
Flame propagation
Lightround
Annular combustion chambers

ABSTRACT

The ignition behaviour of a multiple-burner annular combustion chamber consisting of 12 or 18 bluff-body premixed methane-air swirl burners was investigated experimentally. The study focusses on the mechanism of lightround, namely the burner-to-burner flame propagation. Side visualization of the spreading flame by 5 kHz OH* chemiluminescence showed that propagation from burner to burner did not follow a purely azimuthal direction, but a sawtooth pattern with downstream and sideways motion from one burner to the following, bringing flame to the downstream part of the recirculation zone of the adjacent burner before being convected upstream leading to full burner ignition. This pattern was more pronounced when the burners where fitted with swirlers. Top visualization and image processing were used to quantify the speed of lightround as a function of inter-burner spacing, bulk velocity, equivalence ratio, and swirling feature. It was found that flame spread from burner to burner following two balanced modes of propagation. These are turbulent flame propagation combined with volumetric expansion in the inter-burner region and convection within the next un-ignited burner. The results presented in this paper bring new insights into the ignition of realistic gas turbines.

1. Introduction

The transient process of ignition in gas turbines involves physical complexity and is very rich from a scientific point of view [1,2]. In the event of a flame-out at high altitude, means of restarting an engine must be provided. In addition, the flame must remain stable after its establishment. This ability to relight the engine at high altitude affects the volume, weight, cost and emissions of the combustor as well as the flight envelope. Moreover, the trend towards lean operation required for pollution targets makes flame initiation and growth more difficult. Nowadays, prediction of the stability limits at the design stage of the combustor has become a challenge for gas turbine manufacturers and more research is needed in order to fully understand the phenomenon.

Successful ignition in gas turbines can be divided into four phases [1,2]. The first phase is the initiation of a flame kernel through a spark in a flammable mixture [2–5]. The second phase is propagation of the flame within the burner. The third phase is overall burner ignition characterized by the stabilization of the flame once ignited. Spark ignition of non-premixed flames has been investigated experimentally in various single burner geometries [6–10], and single burner ignition has been studied experimentally [11–13] and numerically with Large Eddy Simulation (LES) [14–19] and low-order models providing simplified and faster ignition modelling [20–22]

Apart from the ignition of single liquid-fuelled gas turbine burners, gas turbine ignition involves additional flame propagation from burner to burner. This phase, denoted lightround corresponds to the last phase of ignition and has not been extensively studied in the laboratory.

In non-premixed mode, Boileau et al. [23] investigated numerically with LES the complete ignition of a full helicopter gas turbine annular combustor. Through this simulation, the mean flow in the azimuthal direction caused by the imbalance between burnt gas production in the flame and its out-flux through the combustion outlet, was identified as a key aspect of the ignition process. Recently, a non-premixed swirl multiple-burner annular combustion chamber has been studied experimentally by Machover and Mastorakos [24]. It was shown that burner-to-burner flame propagation occurring in the stratified inter-burner region consisted of a successful flame propagation event following a succession of failed events in which a flame fragment coming from the ignited burner failed to penetrate fully in the recirculation zone of the adjacent un-ignited burner. The number of failed events appeared to vary

* Corresponding author.
E-mail addresses: edouard.machover@gmail.com (E. Machover), erm42@cam.ac.uk (E. Mastorakos).

http://dx.doi.org/10.1016/j.combustflame.2017.01.013

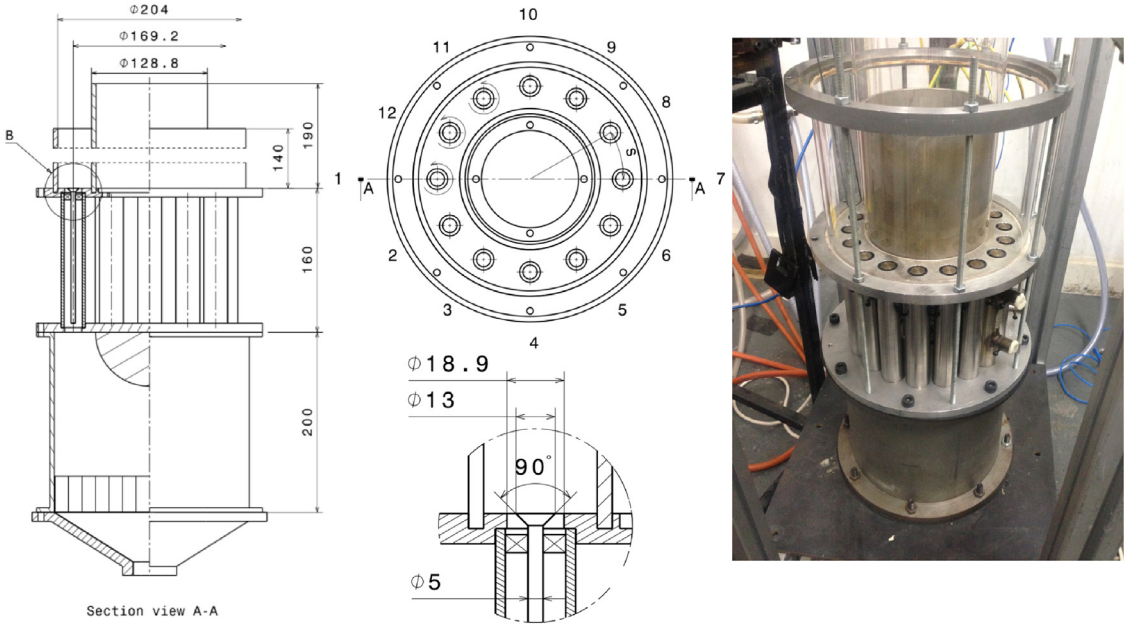

Fig. 1. Drawing of the annular premixed combustor in the 12-burner configuration and photograph of the annular premixed burner assembly. Real dimensions of the enclosure are provided by the drawing. Circular arrows indicate the direction of the swirl. The burners, separated by arc distance S, are numbered counter-clockwise. The dimensions are in mm.

significantly from burner to burner suggesting a stochastic global behaviour. Burner-to-burner flame propagation was then investigated numerically with the low-order ignition model developed by Neophytou et al. together with a probabilistic model developed in order to quantify the stochasticity of the process [25]. The stochastic behaviour of the combustor, the lean lightround ignition limits and the mean lightround speed measured experimentally were explained and accurately predicted, demonstrating the validity of the use of the method developed to predict the ignition behaviour of the combustor.

In premixed mode, were the mixture between burners is flammable everywhere, Bourgouin et al. [26] investigated lightround through lab-scale experiments with an annular combustion chamber consisting of a number of identical swirl premixed burners placed in an annular combustion chamber open to the atmosphere downstream. Bulk velocity was found to have an impact on the speed of lightround with decreasing burner-to-burner propagation time with increasing bulk velocity. The combination of flow motion generated by volumetric expansion across the flame and normal burning velocity was evidenced as controlling flame displacement velocity. Furthermore, the convection of the flame downstream was attributed to the burned gases formed by ignited injectors and by buoyancy forces. These suggestions were supported by numerical simulations based on a modified G-equation and more recently by LES [27–29]. Moreover, a combustion chamber comprising five injectors arranged linearly and considered as premixed in the whole combustion chamber except in the vicinity of the burners has been studied through experiments and simulations with LES by Barré et al. [30]. The impact of the inter-burner spacing on the ignition process was investigated. The authors found that inter-burner spacing had an influence on the burner-to-burner flame propagation as the process of ignition varied from one injector and the subsequent one according to two balanced modes. These modes are spanwise propagation associated with low inter-burner spacing, and streamwise convection by the mean flow associated with higher inter-burner spacings. Spanwise propagation mode was identified as the result of rapid capture of the flame by the swirled motion of the adjacent burner during burner-to-burner propagation. It was found that spanwise propagation was characterized by high speed of lightround and low variability, whereas streamwise propagation mode was associated with lower burner-to-burner propagation speed and higher variability.

In the present work, the physical mechanisms responsible for burner-to-burner flame propagation in premixed mode in annular combustion chambers are investigated experimentally, with emphasis on the speed of lightround. The annular rig used has been studied before from the perspective of thermoacoustic oscillations [31,32]. We extend the previous results by Bourgouin et al. [26] and Barré et al. [30] by studying a wider range of operating conditions in terms of bulk velocity, burner spacing, equivalence ratio, and swirling vs. non-swirling flow. First, the experimental set-up are presented, followed by the experimental results. Finally, the paper concludes on the main mechanisms driving the lightround in premixed annular combustion chambers.

2. Methods

2.1. Premixed annular burner setup

The annular burner is displayed in Fig. 1 and was described in detail by Worth and Dawson in Refs. [31,32]. The apparatus consisted of a number of equally spaced bluff-body stabilized turbulent premixed flames placed in an annular configuration. Methane/air mixtures flowed into a 200 mm long cylindrical plenum chamber with a 212 mm inner diameter 212 mm containing flow straighteners and a series of grids. As each of the flames was fed by reactants from a common plenum, a hemispherical body of diameter $D_h = 140$ mm was positioned inside the plenum to improve flow uniformity. The reactant mixture passed from the plenum into a number of 150 mm long circular tubes with an inner diameter $D = 18.9$ mm. Each tube was fitted with a centrally located conical bluff-body of diameter $d_a = 13$ mm with a half angle of 45° giving a blockage ratio of 50% at the inlet to the combustion chamber. The tubes were arranged around a circle of 169.2 mm diameter and fixed between upper and lower plates. For some measurements, a six vane, $\alpha = 60°$, counter-clockwise removable swirler (as viewed from the top of the combustor) was fitted 10 mm upstream each of the bluff-body giving a calculated geometrical swirl number of 1.22 [31]. The flames were confined within an annular enclosure that consisted of quartz inner and

Table 1
Flow conditions investigated experimentally for the annular premixed burner.

Φ	U_b [m/s]	Swirl	No swirl
12-burner configuration			
0.60	10	Yes	No
0.70	[10:2:18]	Yes	Yes
0.80	[10:2:14]	Yes	No
0.90	[10:2:14]	Yes	No
18-burner configuration			
0.70	[10:2:18]	Yes	Yes

outer tubes of diameter $D_{in} = 128.8$ mm and $D_{out} = 204$ mm of 190 mm and 140 mm lengths, respectively. Two sets of plates were manufactured with the same circumference enabling experiments with 12 and 18 burner configurations to be performed. These correspond to flame separation distances of $S_{12} = 2.33\,D$ ($S = 44.0$ mm) and $S_{18} = 1.56\,D$ ($S = 29.5$ mm), respectively, where S denotes the arc distance between the bluff-body centres.

2.2. Flow conditions and ignition unit

All measurements were carried out in ambient conditions of temperature ($T = 293$ K) and pressure (1 bar), at four equivalence ratios (ϕ=0.6, 0.7, 0.8, 0.9) in the 12-burner configuration and at a single equivalence ratio ($\phi = 0.7$) in the 18-burner configuration, with bulk velocity (U_b) ranging between $U_b = 10$ m/s and $U_b = 18$ m/s with 2 m/s increment (denoted here $U_b = [10:2:18]$ m/s). These velocities, assessed at the annular opening between each bluff-body and its burner, are lower than in realistic gas turbines, but are sufficiently high to produce turbulent flow (the Reynolds number, Re, based on the bulk velocity at each burner's annular inlet and D ranged from $Re = 3800$ to $Re = 6800$). Experiments were also performed without swirl for both inter-burner spacings at $\phi = 0.7$. Flame propagation was observed at each equivalence ratio (the flammability limits for premixed air/methane mixtures are 0.46 (poor) and 1.64 (rich) [33]) The flow rates of air and methane (99.96% pure) were controlled by Alicat mass flow controllers. Measurements were performed after the combustor had been ignited for times long enough to allow the combustor to operate in steady-state regime. Hence, all the experiments have been carried out under hot conditions, in the sense that the walls were relatively hot after the combustor being run with flame for some time before being switched off for the ignition experiments. A flame characterized by inter-burner spacing S, equivalence ratio ϕ and bulk velocity U_b is denoted flame $S\_\phi\_U_b$. Without swirl, the denomination flame $S\_\phi\_U_b\_ws$ is used. In the present work, when a flame parameter is changed, the others are kept constant. The conditions are summarized in Table 1.

The electrical spark system has been used in previous studies [6,7]. Two free tungsten electrodes with pointed ends of 1 mm diameter and 2 mm gap from each other were placed at location $(z/d_a,\ r/d_a) = (1.7,\ 0.0)$, where the Cartesian coordinate system is fixed at the centre of the bluff-body at the first burner exit plane. The electrical unit deposited very repeatable sparks [7] of 0.4 ms duration and 140 mJ energy. This energy was much higher than the minimum ignition energy for methane/air mixtures at the equivalence ratios used [5].

2.3. Chemiluminescence measurements and analysis technique

The ignition transient was recorded with fast imaging (5 kHz) of OH* chemiluminescence. A LaVision HighSpeed IRO two stage intensifier with a spectral range of 190–800 nm gated at 190 μs at 5 kHz was coupled to a Photron Fastcam SA1.1 monochrome high speed CMOS camera with 1024 × 1024 pixels resolution up to 5.4 kHz fitted with a UV bandpass filter (270–370 nm). In order to protect the intensifier from the possibility of intense emission from the spark, a triggering system was used such that the acquisition started once the spark had ended. The overall time taken to ignite the combustor was calculated by analysing chemiluminescence movies, taken from the top of the combustion chamber, of the flame as it progresses round the annular combustion chamber. In order to protect the camera from the hot exhaust gases, the movies were enabled by fitting an air-cooled 45° angle from the vertical mirror downstream of the combustor, as shown schematically in Fig. 2.

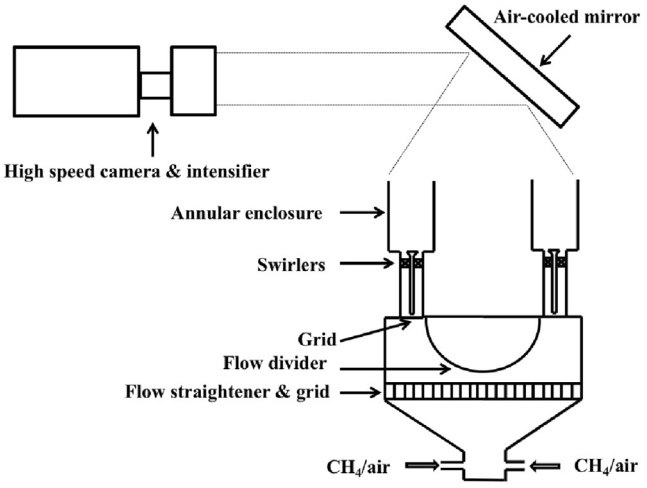

Fig. 2. Side schematics of the annular burner and imaging set-up.

In order to quantify the flame evolution in the annular combustor, the films where post-processed in the following way. First, the movies taken from the top of the combustion chamber were decomposed into images according to the frame rate of the camera. These images were then converted into black and white by a thresholding procedure so that the pixels with a certain amount of light intensity greater than that of the one of the threshold were considered as ignited while those with light intensity below were considered as non-ignited. Then, a mask has been implemented to all the images so that only the area within the boundaries of the annular rig was taken into account (i.e., $\pi\,({D_{out}}^2 - {D_{in}}^2)/4)$). The burner-to-burner flame propagation speed was estimated by monitoring the rate of growth of the number of pixels denoting inflamed area as a percentage of the whole annulus number of pixels.

3. Results and discussion

3.1. Ignition visualization

A photograph of three ignited swirling burners is shown in Fig. 3. A series of individual flames, each attached to a bluff-body, is apparent. The flames merge in the region between the burners and impinge on both, the inner and outer enclosures. In the case of Fig. 3, each of the individual burners was fitted with a swirler, which changes the aerodynamics relative to the un-swirled bluff-body flows. The flames are not stabilized neither in the wakes formed by the sudden expansion between two burners nor between the burners and the enclosures. Instead, it appears to be stabilized only at the edge of the bluff-bodies.

An example of the steady swirling flame as seen from the top of the combustor is shown in Fig. 4. Some individual burners and the counter-clockwise direction of the swirl have been added schemat-

Fig. 3. Photograph of flame 12_0.70_10.

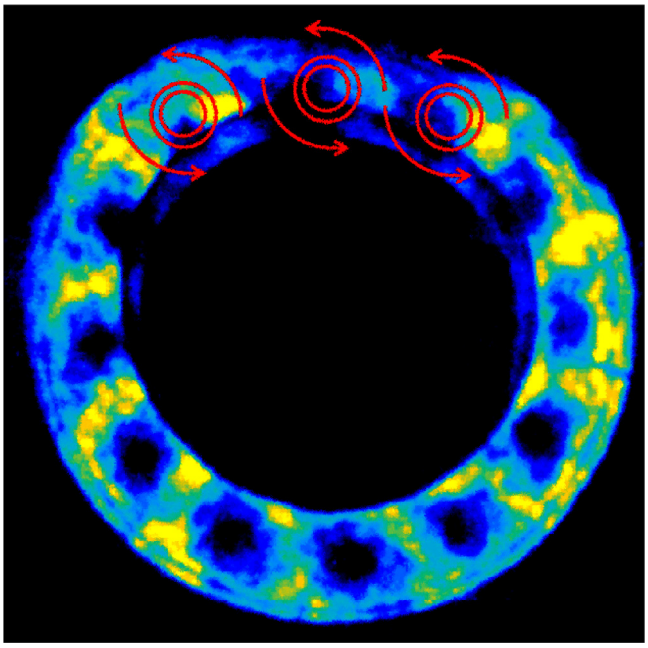

Fig. 4. Top view of the steady-state flame with swirl. Single OH* chemiluminescence snapshot. Flame 12_0.70_12.

ically. The steady flame is composed of a series of 12 cylindrical flames associated to each burner, with no chemiluminescence emission from the region immediately downstream of the bluff-bodies. Flames attached to the burners show a slightly skewed shape resulting from the counter-clockwise tangential component of the velocity induced by the swirl along the outer wall of the combustion chamber and the clockwise velocity component along the inner enclosure of the combustor.

The burner-to-burner propagation mechanism with swirl is visible in Fig. 5 where a sequence of two successful flame propagations from burner to burner in the 12-burner configuration is shown. A sawtooth movement from burner to burner is the prevailing propagation pattern; it occurs in two steps and is associated with a timescale τ_T. The downstream edge of the first flame is first convected away and grows on the side of the next burner. An azimuthal and downstream movement resulting from convection by the fast flow coming out from the annular expanding air/gas inlet and from flame propagation is visible. This movement occurs over a timescale τ_D. The adjacent burner is then ignited by its own recirculation zone (RZ), capturing a flame fragment from downstream. The flame is quickly convected upstream towards the bluff body and spreads to fill the whole recirculation zone, leading to full burner ignition. Ignition of the burner is associated with a timescale τ_U, such that $\tau_T = \tau_D + \tau_U$. Since the OH* chemiluminescence imaging is line-of-sight, from the top view it is not clear if this movement is across the two merging annular jets formed by the expanding flow at the sides of each bluff-body, or if the flame bypasses the burner by igniting temporarily the region between the burner and the enclosure. Flow over the side view (Fig. 5) clearly shows this sawtooth pattern that is consistent with the key mechanisms of ignition of a single burner with recirculation zone [1,6,20,22].

The burner-to-burner propagation mechanism without swirl is visible in Fig. 6. Successive adjacent burners are ignited by flame propagation along the lower wall between burners, and the sawtooth pattern is less pronounced. In the inter-burner region, the flame propagates in the azimuthal direction before being captured by the next burner's RZ.

These results obtained with and without swirl show that the ignition process evolves from burner to burner with a balance between flame propagation along the flammable mixture between burners in the cross-flow direction and convection by the mean flow in the axial direction, which is consistent with results obtained with swirling flames by Barré et al. [30].

3.2. Time of complete ignition and flame speed

Burner-to-burner flame propagation as seen from the top of the annular combustor is shown in Fig. 7. For every flame considered, the flame front across the annular opening is skewed; it propagates along the outer wall further than along the inner wall at the lower part of the images, while it propagates faster along the inner enclosure at the top part of the images. This is due to the counter-clockwise swirling pattern from each burner (as viewed from the top of the combustion chamber) that induces velocity components along the walls of the annular combustor, which results in pushing the flame accordingly. Moreover, the flame front propagates faster in the clockwise direction, which can be attributed to shorter flame travelling distance from burner-to-burner at low radius (i.e., close to D_{in}) within the combustion chamber, where swirl induces a clockwise tangential velocity component.

The effects of inter-burner spacing and bulk velocity on flame propagation were investigated by varying S and U_b, at an equivalence ratio fixed to 0.7. In both 12 and 18-burner configurations, increasing bulk velocity, at fixed ϕ and S, results in an increase of the speed of lightround (e.g., at $t = 30$ ms, the flame fronts have merged for flames 12_0.7_18 and 18_0.7_18, whereas flame propagation is still occurring for flames 12_0.7_10 and 18_0.7_10). Furthermore, reducing the spacing between burners at fixed ϕ and U_b, results in speed of lightround decrease (e.g., the flame fronts merge at $t = 24$ ms for flame 12_0.7_18 whereas they merge between $t = 24$ ms and $t = 30$ ms for flame 18_0.7_18). Given that the time required for the combustor to be fully ignited is approximately the same for flame 18_0.7_10 and for flame 12_0.7_10, we conclude that an increase in bulk velocity has a much larger effect on burner-to-burner propagation speed when the inter-burner spacing is higher. However, the snapshots presented in Fig. 7 show single ignition events; accurate conclusions concerning speed of lightround can only be drawn through observation of many realizations compiled in order to determine the average behaviour of the combustor.

In order to quantify the burner-to-burner flame propagation speed, the ignited annular area expressed as a percentage of the area of the annular chamber, as viewed from the top of the combustion chamber, is plotted vs. time in Fig. 8 for all flames shown in Fig. 7. The lightround speed, being dependent on the direction the flame moves, is calculated as an average of that from

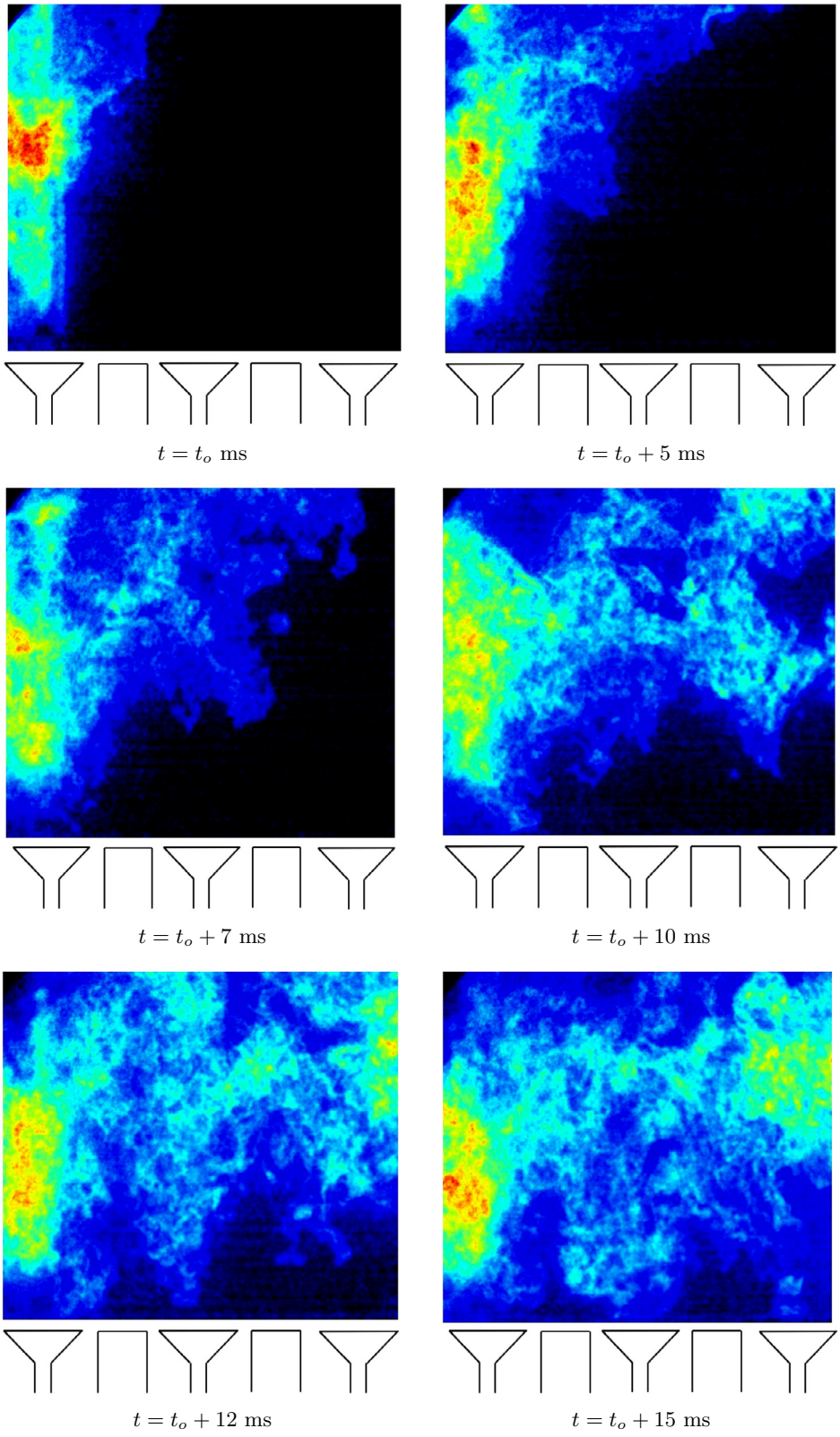

Fig. 5. Side visualization by 5 kHz OH* chemiluminescence of evolution of a successful burner-to-burner flame propagation for flame 12_0.70_10. A succession of three burners is sketched.

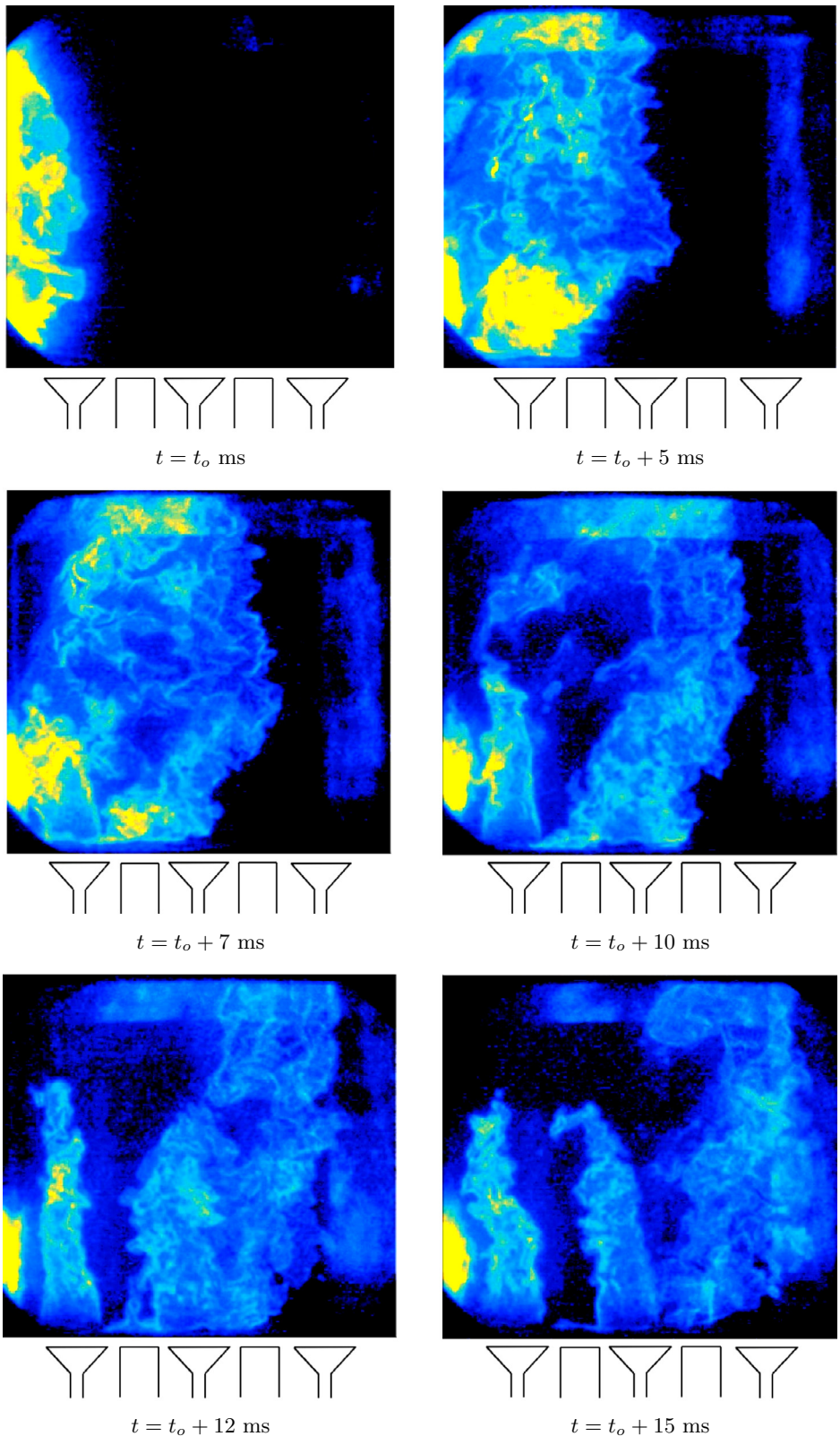

Fig. 6. Side visualization by 5 kHz OH^* chemiluminescence of evolution of a successful burner-to-burner flame propagation for flame 12_0.70_10_ws. A succession of three burners is sketched.

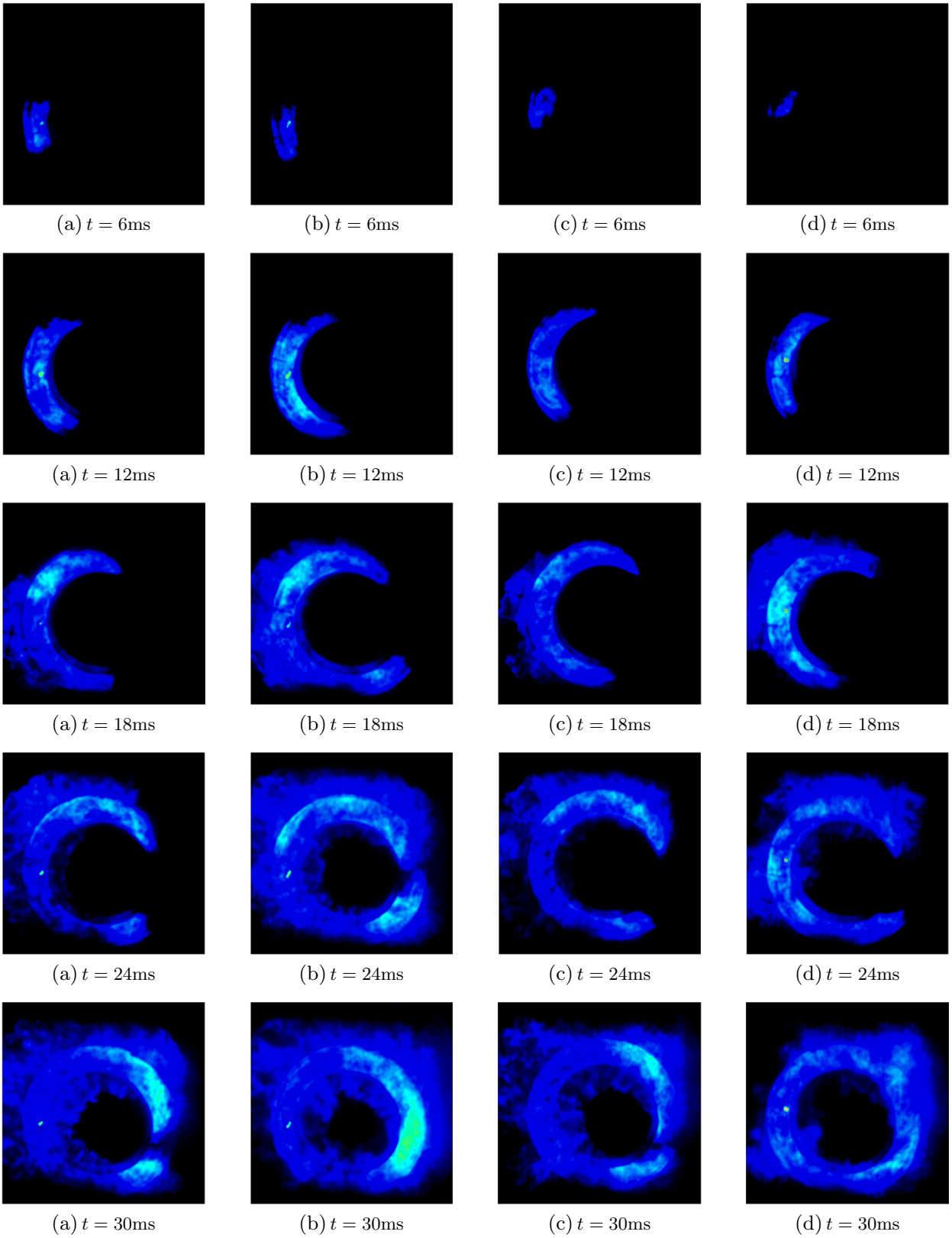

Fig. 7. Top visualization by 5 kHz OH^* chemiluminescence of flame evolution in the annular combustor for flames (a) 12_0.7_10, (b) 12_0.7_18, (c) 18_0.7_10 and (d) 18_0.7_18.

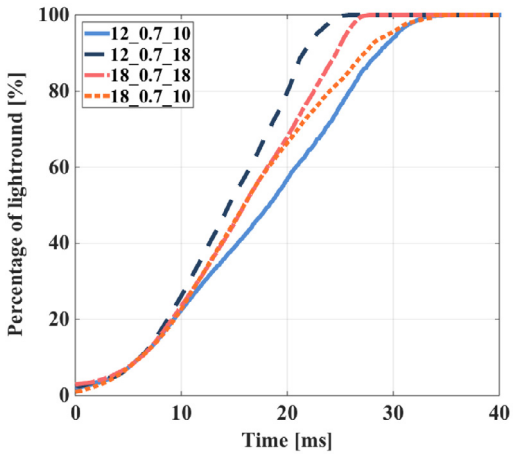

Fig. 8. Fraction of annular combustor area ignited vs. time for flames 12_0.7_10, 12_0.7_18, 18_0.7_10 and 18_0.7_18. The curves show average values of four separate ignition events.

both clockwise and counter-clockwise branches of the flame. For each flame, the average of four individual movies is shown. There is slow initial evolution associated with the time required to ignite the first burner. Subsequently, the opposite flames travel from burner to burner at a rather constant speed, which is shown by the linear slopes of the fraction of annular combustor area ignited vs. time, until the flame fronts are close to merging. At the end of the process, the merging results in a lightround speed reduction.

The time of complete combustor ignition varies somewhat between individual spark events, variability being related to that of the first burner as shown in Fig. 9. The variability increases with a decrease in the inter-burner spacing (Fig. 9a), bulk velocity (Fig. 9b), equivalence ratio, (Fig. 9c) and with the removal of swirl (Fig. 9d).

For all the flow conditions summarized in Table 1, the average speed of lightround (S_{LR}) was obtained by multiplying the slope of the curve of the percent-ignited combustor vs. time by the half-perimeter of the combustor (i.e., calculated at a radius half-way between inner and outer walls). Slopes were calculated for values comprised between 20 and 80% complete burner ignition rates, (i.e., during flame steady growth), in order to avoid edge effects due to first burner ignition and flame fronts merging.

For swirling flames, the dependence of burner-to-burner average propagation speed with bulk velocity for both inter-burner spacings is shown in Fig. 10. Assuming a typical turbulence intensity u' of about 20% of the bulk velocity in these swirling recirculating flows [34], the ratio u'/S_L, where S_L denotes the laminar flame speed, is approximately equal to 10 for $U_b = 10$ m/s and equal to 18 for $U_b = 18$ m/s. Consequently, the ratio S_T/S_L, where S_T denotes the turbulent flame speed, is expected to increase with u'/S_L, albeit less than linearly. The ratio between the lightround speeds measured experimentally at $U_b = 18$ m/s and at $U_b = 10$ m/s varies depending on the inter-burner spacing (this ratio is equal to 1.4 between flame 12_0.7_18 and flame 12_0.7_10 whereas it is equal to 1.1 between flame 18_0.7_18 and flame 18_0.7_10). This suggests that flame propagation along the azimuthal direction is not only related to the turbulent flame propagation but also to other factors such as local quenching and local convection patterns, especially when the inter-burner spacing is reduced, which supports previous suggestions based on LES [23] and the single-burner ignition investigation described by Neophytou et al. [20].

We restrict herein the study on propagation from one ignited burner to the adjacent un-ignited burner occurring in τ_T, where U_{LR} denotes the local speed of the flame front during the lightround process. F_D and F_U denote the timed average speed of propagation in the inter-burner region and in the burner region, respectively. U_{LR} can be written as:

$$\forall t \in [0, \tau_T], U_{LR}(t) = \begin{cases} F_D & t \in [0, \tau_D] \\ F_U & t \in [\tau_D, \tau_T]. \end{cases}$$

The average speed of lightround, S_{LR} is by symmetry the time average of U_{LR} over τ_T:

$$S_{LR} = \overline{U_{LR}} = \frac{1}{\tau_T}\int_0^{\tau_T} U_{LR}(t)\,\mathrm{d}t = \frac{1}{\tau_T}\left(\int_0^{\tau_D} F_D\,\mathrm{d}t + \int_{\tau_D}^{\tau_T} F_U\,\mathrm{d}t\right). \quad (1)$$

Finally, given that F_D and F_U are constant over time since these quantities denote time-averaged speeds of propagation, S_{LR} can be written as:

$$S_{LR} = \frac{\tau_D}{\tau_T}F_D + \frac{\tau_U}{\tau_T}F_U. \quad (2)$$

Hence, the speed at which flame propagates from an ignited burner to the next un-ignited one during time τ_T can be estimated as the sum of two functions. The first function F_D represents the average speed of propagation in the inter-burner region. It is weighted by the ratio τ_D/τ_T in order to take into account the relative importance of the inter-burner propagation in the total burner-to-burner propagation process. F_D is an increasing function of bulk velocity in that an increase in U_b leads to higher level of turbulence favouring faster turbulent propagation, and to faster convection of the flame by the annular flow in the inter-burner region (mostly in the swirling cases). The second function F_U is the average speed of burner ignition. It is weighted by the ratio τ_U/τ_T to consider the relative importance of the flame convection within the RZ of each burner. F_U is a decreasing function of bulk velocity (the fact that at high U_b each burner may take longer to fully ignite has been evidenced in [22]). Indeed, an increase of U_b has a detrimental effect on ignition of the next adjacent burner given that the flame has to move upstream opposite to direction of flow, in order to ignite the RZ as evidenced by side imaging.

For both inter-burner spacings, increasing U_b results in an increase of S_{LR}, a trend consistent with the observations reported in [26]. Increasing relationship between S_{LR} and U_b is explained by the dominance of the first term over the second in Eq. (2). Moreover, faster growth of S_{LR} with U_b in the 12-burner configuration than in the 18-burner configuration is explained by an increase of the weighting of the second term in Eq. (2) with inter-burner spacing increase. The timescale of burner ignition τ_D as a proportion of the total time of propagation $\tau_T = \tau_D + \tau_U$ decreases with a reduction in inter-burner spacing.

For non-swirling flames, Fig. 10 shows the lightround speed as a function of bulk velocity for both inter-burner spacings. Removing swirl results in decrease of S_{LR} for every flame considered, which is explained by lower turbulence levels than with swirl, leading to turbulent flame propagation speed reduction. Similarly to the swirling case, a growing relationship between S_{LR} and U_b for both inter-burner spacings is evidenced. However, an increase in U_b leads to a smaller increase of S_{LR} than with swirling flames, which is explained by the lower value of the first term of Eq. (2) resulting from the u' decrease. Furthermore, an increase in number of burners results in lightround speed decrease which is explained, as in the swirling case, by a reduction of the inter-burner region where turbulent flame propagation occurs. S_{LR} remains rather constant with U_b increase in the 18-burner configuration, which shows that, in Eq. (2), a decrease of first term compensates the increase of second term as U_b increases.

Figure 9c shows that increase of ϕ results in increase of S_{LR}. This confirms the mechanism of turbulent propagation in the inter-burner region, given that an increase in equivalence ratio results in an increase in S_L, and subsequent increase of turbulent flame speed. Furthermore, the ratio S_{LR}/S_L evolves continuously

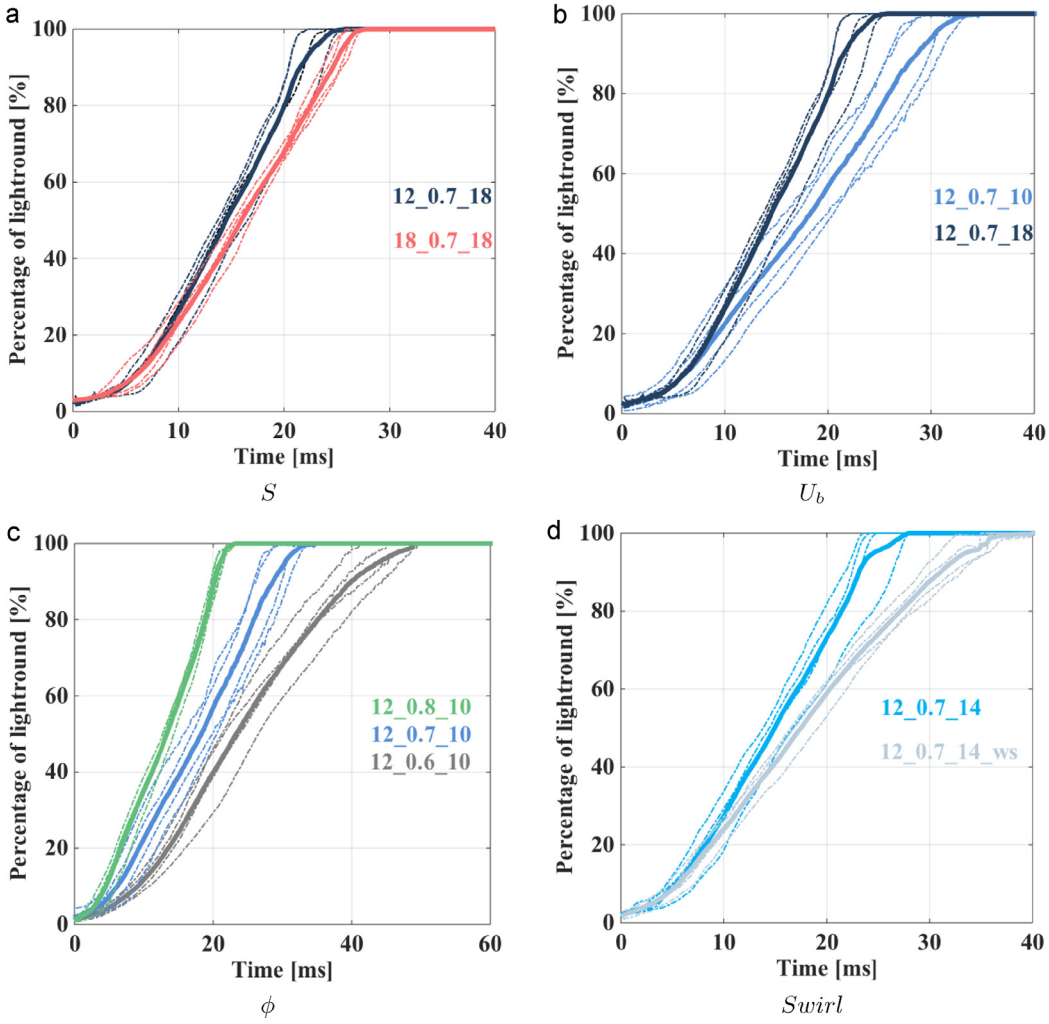

Fig. 9. Fraction of annular combustor area ignited vs. time. For each flame, four separate ignition events (fine dotted lines) and their average (thick solid lines) are shown.

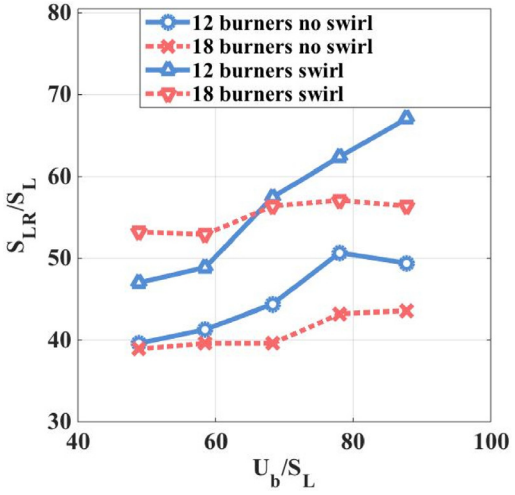

Fig. 10. Experimental speeds of lightround as a function of the bulk velocity and inter-burner spacing, with swirl (a), and without swirl (b). Equivalence ratio is fixed at 0.7. All speeds are normalized by the laminar flame speed at $\phi = 0.7$ [37].

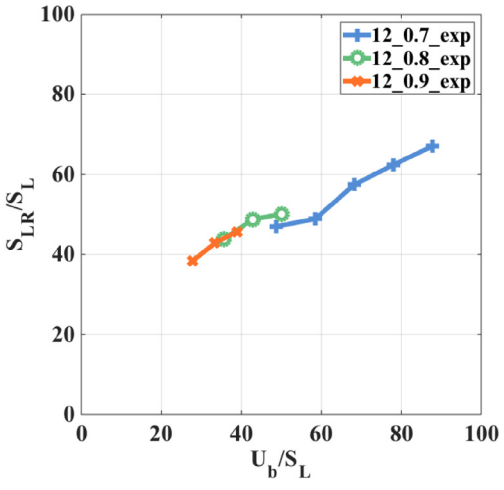

Fig. 11. Experimental speeds of lightround as a function of the bulk velocity for three equivalence ratios. Number of burners is fixed at 12. All speeds are normalized by the laminar flame speed at the equivalence ratio considered [37].

and monotonously with U_b/S_L, regardless of ϕ (Fig. 11), which illustrates the role of the turbulent propagation mechanism in the combustion chamber. This result should be confirmed with other evidence such as flame wrinkling for example. Moreover, the comparison of the slopes of the curves in Fig. 11 and that, showing the evolution of the ratio S_T/S_L over the ratio u'/S_L [22], show that at

every equivalence ratio considered, the flame propagates at speed close to θS_T, where $\theta = \rho_u/\rho_b$ and ρ_u and ρ_b are the densities of the unburned and burnt gases, respectively (values of θ are equal to 6.3, 6.8 and 6.9 for $\phi = 0.7$, $\phi = 0.8$ and $\phi = 0.9$, respectively [35]). These results confirm volumetric expansion within the flow together with turbulent propagation as described in [10,26,36].

4. Conclusions

The ignition behaviour of an annular combustion chamber, comprising 12 or 18 individual bluff-body premixed burners, has been examined experimentally and in order to understand the way a flame propagates from burner to burner.

Side high-speed imaging of the flame as it progressed in the combustion chamber showed that the ignition process evolved from burner to burner with a balance between two modes. These are turbulent propagation across the regions between the burners and a sawtooth pattern, the latter mode consisting in a succession of upstream movement by the expanding annular flow inlet and downstream movement from the top of the recirculation zone of the adjacent un-ignited burner.

These results were confirmed by top flame imaging allowing quantification of the evolution of the burner-to-burner propagation speed with variations in swirling feature, inter-burner spacing, overall equivalence ratio and bulk velocity. Adding swirl, increasing bulk velocity or increasing equivalence ratio resulted in increase of speed of lightround. Decrease in inter-burner spacing resulted in smaller impact of bulk velocity increase on lightround speed. Moreover, the variation of the lightround speed with bulk velocity at several equivalence ratios showed that flame acceleration across the flame front due to variation in density played a important role in the turbulent flame displacement speed.

In the present experiments, the mixture fraction is homogeneous everywhere, and the fluid occupying the inter-burner region is flammable, which allows propagation across the burners. However, burner-to-burner flame propagation is more complex in liquid-fuelled systems or with radial fuel staging burners due to uneven equivalence ratio distribution across the combustion chamber. This implies that the region between burners may not be flammable (see Ref. [24] for the study of the global lightround behaviour of an annular non-premixed combustor). Study of premixed systems is a useful first step in understanding the realistic gas turbine ignition problem.

Supplementary material

Supplementary material associated with this article can be found, in the online version, at 10.1016/j.combustflame.2017.01.013.

Acknowledgments

We thank Dr. Nick Worth for assistance with the experiments and useful discussions. The authors acknowledge financial assistance from EPSRC and Rolls–Royce Group.

References

[1] E. Mastorakos, Ignition of turbulent non-premixed flames, Prog. Energy Combust. Sci. 35 (2009) 57–97.
[2] A.H. Lefebvre, Gas turbine combustion, 2nd ed., Taylor and Francis, London, 1999.
[3] I. Glassman, R.A. Yetter, Combustion, 4th ed., Academic Press, San Diego, California, USA, 2008.
[4] D.B. Spalding, Combustion and mass transfer, Pergamon Press, Oxford, UK, 1979.
[5] B. Lewis, G.V. Elbe, Combustion, flames and explosions of gases, Harcourt Brace Jovanovich, London, 1987.
[6] S.F. Ahmed, R. Balachandran, T. Marchione, E. Mastorakos, Spark ignition of turbulent nonpremixed bluff-body flames, Combust. Flame 151 (2007) 366–385.
[7] S.F. Ahmed, E. Mastorakos, Spark ignition of lifted turbulent jet flames, Combust. Flame 146 (2006) 215–231.
[8] S.F. Ahmed, R. Balachandran, E. Mastorakos, Measurements of ignition probability in turbulent non-premixed counterflow flames, Proc. Combust. Inst. 31 (2007) 1507–1513.
[9] S.F. Ahmed, E. Mastorakos, Correlation of spark ignition with the local instantaneous mixture fraction in a turbulent nonpremixed methane jet, Combust. Sci. Technol. 182 (2010) 1360–1368.
[10] S.F. Ahmed, E. Mastorakos, Spark ignition of a turbulent shear-less fuel-air mixing layer, Fuel 164 (2016) 297–304.
[11] R.W. Read, J.W. Rogerson, S. Hochgreb, Flame imaging of gas-turbine relight, AIAA J. 48 (2010) 1916–1927.
[12] T. Mosbach, R. Sadanandan, W. Meier, R.L.G.M. Eggels, Experimental analysis of altitude relight under realistic conditions using laser and high-speed video techniques, Proceedings of the ASME Turbo Expo 2010, vol. 2, Combustion, Fuels and Emissions, Parts A and B, Glasgow, UK (2010), pp. 523–532.
[13] A. Lang, R. Lecourt, F. Giuliani, Statistical evaluation of ignition phenomena in turbojet engines, Proceedings of the ASME Turbo Expo 2010, 48, Glasgow, UK (2010), pp. 985–992.
[14] G. Lacaze, E. Richardson, T. Poinsot, Large eddy simulation of spark ignition in a turbulent methane jet, Combust. Flame 156 (2009) 1993–2009.
[15] A. Triantafyllidis, E. Mastorakos, R.L.G.M. Eggels, Large eddy simulation of forced ignition of a non-premixed bluff-body methane flame with conditional moment closure, Combust. Flame 156 (2009) 2328–2345.
[16] V. Subramanian, P. Domingo, L. Vervisch, Large eddy simulation of forced ignition of an annular bluff-body burner, Combust. Flame 157 (2010) 579–601.
[17] W.P. Jones, V.N. Prasad, LES-pdf simulation of a spark ignited turbulent methane jet, Proc. Combust. Inst. 33 (2011) 1355–1363.
[18] W.P. Jones, A.J. Marquis, V.N. Prasad, LES of a turbulent premixed swirl burner using the Eulerian stochastic field method, Combust. Flame 159 (2012) 3079–3095.
[19] G. Bulat, W.P. Jones, A.J. Marquis, Large eddy simulation of an industrial gas–turbine combustion chamber using the sub-grid PDF method, Proc. Combust. Inst. 34 (2013) 3155–3164.
[20] A. Neophytou, E.S. Richardson, E. Mastorakos, Spark ignition of turbulent recirculating non-premixed gas and spray flames: a model for predicting ignition probability, Combust. Flame 159 (2012) 1503–1522.
[21] A. Eyssartier, B. Cuenot, L.Y.M. Gicquel, T. Poinsot, Using LES to predict ignition sequences and ignition probability of turbulent two-phase flames, Combust. Flame 160 (2013) 1191–1207.
[22] M.P. Sitte, E. Bach, J. Kariuki, H.-J. Bauer, E. Mastorakos, Simulations and experiments on the ignition probability in turbulent premixed bluff-body flames, Combust. Theory Model. 20 (2016) 548–565.
[23] M. Boileau, G. Staffelbach, B. Cuenot, T. Poinsot, C. Berat, LES of an ignition sequence in a gas turbine engine, Combust. Flame 154 (2008) 2–22.
[24] E. Machover, E. Mastorakos, Spark ignition of annular non-premixed combustors, Exp. Therm. Fluid Sci. 73 (2016) 64–70.
[25] E. Machover, Spark ignition in annular combustors, University of Cambridge, 2016 Ph.D. thesis.
[26] J.-F. Bourgouin, D. Durox, T. Schuller, J. Beaunier, S. Candel, Ignition dynamics of an annular combustor equipped with multiple swirling injectors, Combust. Flame 160 (2013) 1398–1413.
[27] M. Philip, M. Boileau, R. Vicquelin, E. Riber, T. Schmitt, B. Cuenot, D. Durox, S. Candel, Large eddy simulations of an annular multiple-injector combustor, Proc. Combust. Inst. 35 (2015) 3159–3166.
[28] M. Philip, M. Boileau, R. Vicquelin, T. Schmitt, D. Durox, J.F. Bourgouin, S. Candel, Ignition sequence in a multi-injector combustor, Phys. Fluids 26 (2014), doi:10.1063/1.4893452.
[29] M. Philip, M. Boileau, R. Vicquelin, T. Schmitt, D. Durox, J.F. Bourgouin, S. Candel, Ignition sequence in a multi-injector combustor, J. Eng. Gas Turbines Power (ASME) 137 (2015) 3.
[30] D. Barré, L. Escalpez, M. Cordier, E. Riber, B. Cuenot, G. Staffelbach, B. Renou, A. Vandel, L. Gicquel, G. Cabot, Flame propagation in aeronautical swirled multi-burners: experimental and numerical investigation, Combust. Flame 161 (2014) 2387–2405.
[31] N.A. Worth, J.R. Dawson, Modal dynamics of self-excited azimuthal instabilities in an annular combustion chamber, Combust. Flame 160 (2013a) 2476–2489.
[32] N.A. Worth, J.R. Dawson, Self-excited circumferential instabilities in a model annular gas turbine combustor: global flame dynamics, Proc. Combust. Inst. 34 (2013b) 3127–3134.
[33] D. Dunn-Rankin, Lean combustion: technology and control, 1st ed., Academic Press, Irvine, California, USA, 2008.
[34] J. Kariuki, J.R. Dawson, E. Mastorakos, Measurements in turbulent premixed bluff body flames close to blow-off, Combust. Flame 159 (2012) 2589–2607.
[35] T. Poinsot, D. Veynante, Theoretical and numerical combustion, 2nd ed., R T Edwards, Inc., Philadelphia, Pennsylvania, USA, 2005.
[36] D. Bradley, M.Z. Haq, R.A. Hicks, T. Kitagawa, M. Lawes, C.G.W. Sheppard, R. Wooley, Turbulent burning velocity, burned gas distribution, and associated flame surface definition, Combust. Flame 133 (2003) 415–430.
[37] C.K. Law, A compilation of experimental data on laminar burning velocities, Reduced Kinetic Mechanisms for Applications in Combustion Systems, Springer, Berlin, Germany, 1993.